Mechanism of *Staphylococcus aureus* peptidoglycan *O*-acetyltransferase A as an *O*-acyltransferase

Carys S. Jones[a], Alexander C. Anderson[a], and Anthony J. Clarke[a,b,1]

[a]Department of Molecular and Cellular Biology, University of Guelph, Guelph, ON N1G 2W1, Canada; and [b]Department of Chemistry and Biochemistry, Wilfrid Laurier University, Waterloo, ON N2L 3C5, Canada

Edited by Suzanne Walker, Harvard Medical School, Boston, MA, and approved July 23, 2021 (received for review February 22, 2021)

The O-acetylation of exopolysaccharides, including the essential bacterial cell wall polymer peptidoglycan, confers resistance to their lysis by exogenous hydrolases. Like the enzymes catalyzing the O-acetylation of exopolysaccharides in the Golgi of animals and fungi, peptidoglycan *O*-acetyltransferase A (OatA) is predicted to be an integral membrane protein comprised of a membrane-spanning acyltransferase-3 (AT-3) domain and an extracytoplasmic domain; for OatA, these domains are located in the N- and C-terminal regions of the enzyme, respectively. The recombinant C-terminal domain ($OatA_C$) has been characterized as an SGNH acetyltransferase, but nothing was known about the function of the N-terminal AT-3 domain ($OatA_N$) or its homologs associated with other acyltransferases. We report herein the experimental determination of the topology of *Staphylococcus aureus* $OatA_N$, which differs markedly from that predicted in silico. We present the biochemical characterization of $OatA_N$ as part of recombinant OatA and demonstrate that acetyl-CoA serves as the substrate for $OatA_N$. Using in situ and in vitro assays, we characterized 35 engineered OatA variants which identified a catalytic triad of Tyr-His-Glu residues. We trapped an acetyl group from acetyl-CoA on the catalytic Tyr residue that is located on an extracytoplasmic loop of $OatA_N$. Further enzymatic characterization revealed that *O*-acetyl-Tyr represents the substrate for $OatA_C$. We propose a model for OatA action involving the translocation of acetyl groups from acetyl-CoA across the cytoplasmic membrane by $OatA_N$ and their subsequent intramolecular transfer to $OatA_C$ for the O-acetylation of peptidoglycan via the concerted action of catalytic Tyr and Ser residues.

peptidoglycan | O-acetylation | *O*-acylransferase | acyltransferase 3 family | *Staphylococcus aureus*

The O-acetylation of cell wall and extracellular polysaccharides is a common theme in nature for their protection from lysis and degradation. Examples include the sialic acid residues of glycoproteins that comprise the glycocalyx of eukaryotic cells (1), xylan of the secondary cell walls of plants (2), and the peptidoglycan (PG), secondary cell wall polysaccharides and biofilm components (e.g., cellulose, alginate) of bacterial cell walls or extracellular matrices (3, 4). PG is an essential component of bacterial cell walls, contributing to both cell shape and protection. Although over 50 chemotypes of PG have been identified (5), the glycan structure is conserved among bacteria. It is composed of repeating units of β-1,4–linked *N*-acetylglucosaminyl (GlcNAc) and *N*-acetylmuramoyl residues (MurNAc), and adjacent glycan strands are cross-linked together through peptides that stem from MurNAc residues.

PG O-acetylation occurs at the C-6 hydroxyl of MurNAc residues in both gram-positive and gram-negative bacteria (reviewed in ref. 6). Though rare, it can also occur at GlcNAc residues, such as in some lactobacilli (7). Initially described in 1958 (8), this modification is now known to occur in a large number of bacteria, particularly pathogens. For example, in a comprehensive study of the staphylococci, only pathogenic species (including *Staphylococcus aureus*) were found to produce O-acetylated PG (9). O-acetylation is a nonstoichiometric modification, and its extent can range from 20 to 70% depending on the organism, environmental conditions, and age of the culture (10–12). With *Enterococcus faecalis*, for example, PG O-acetylation levels increase by 10 to 40% as cultures enter the stationary phase and a further 10 to 16% as cells enter the viable but nonculturable state (13). It is not yet known with any bacterium if the *O*-acetyl moieties are dispersed throughout the PG sacculus or localized to particular regions (6).

The main pathobiological role of PG O-acetylation is the inhibition of lysozyme, an enzyme of the innate immunity system that hydrolyzes the glycosidic linkage between MurNAc and GlcNAc residues causing bacterial cells to lyse. The C-6 hydroxyl of MurNAc is important for the coordination of PG into the substrate-binding cleft of lysozyme (14) and so its O-acetylation sterically hinders this interaction (15, 16). With *Listeria monocytogenes*, in addition to providing resistance to lysozyme, PG O-acetylation is important for its growth in macrophages, conferring resistance to bacteriocins and β-lactam antibiotics and limiting the innate immune response (17). The ability of PG O-acetylation to modulate the immune system is of particular interest, as during *S. aureus* infection, the O-acetylation of PG limits T helper cell priming required to develop an effective protective response to systemic infection (18). Hence, PG O-acetylation is considered important for virulence in this (18–20) and numerous other pathogens (21), including *L. monocytogenes* (17), *Streptococcus pneumoniae* (22), *E. faecalis* (23), *Neisseria meningitidis* (24), *Neisseria gonorrhoeae* (25, 26), and *Helicobacter pylori* (27).

As with other cell wall and many glycocalyx components, the O-acetylation of PG is a postbiosynthetic modification. It occurs after the incorporation of GlcNAc-MurNAc-pentapeptide (Lipid II) precursors into the existing sacculus (28–31). Accordingly,

Significance

Enzymes comprised of membrane-spanning acyltransferase-3 (AT-3) domains catalyze the O-acetylation of diverse extracytoplasmic glycans in all forms of life. In many cases, such as peptidoglycan, these glycans represent important cell wall components, and their O-acetylation confers resistance to lytic enzymes. The enzyme responsible for peptidoglycan O-acetylation in gram-positive bacteria, OatA, is a single bimodal protein of an AT-3 domain fused to an SGNH domain. The AT-3 domain adopts a different topology to that predicted in silico. Moreover, its utilization of a unique mechanism for the translocation of acetyl groups across the cytoplasmic membrane for their transfer to peptidoglycan involving catalytic Tyr and Ser residues may be broadly applicable to homologs involved in the modification of other important cell wall glycans.

Author contributions: C.S.J. and A.J.C. designed research; C.S.J. and A.C.A. performed research; C.S.J., A.C.A., and A.J.C. analyzed data; and C.S.J. and A.J.C. wrote the paper.

The authors declare no competing interest.

This article is a PNAS Direct Submission.

[1]To whom correspondence may be addressed. Email: ajclarke@wlu.ca.

This article contains supporting information online at https://www.pnas.org/lookup/suppl/doi:10.1073/pnas.2103602118/-/DCSupplemental.

Published September 3, 2021.

acetyl groups must therefore be translocated across the cytoplasmic membrane from a cytoplasmic donor to the cell wall. Two distinct enzymatic systems have been identified in bacteria for this purpose, both of which are now thought to be the ancestors for homologous systems that evolved in eukaryotes (2). The system operating in gram-positive bacteria, which was first discovered in *S. aureus* (20), is analogous to those involved with the O-acetylation of exopolysaccharides in the Golgi of animals and fungi (2). In each of these cells, a single bimodal protein (named *O*-acetyltransferase A [OatA] in gram-positive bacteria) is postulated to catalyze both the translocation and transfer reactions. With OatA, its N-terminal domain ($OatA_N$) is predicted to be a member of Acyl_transf_3 (AT-3) Acyltransferases (pfam PF01757; InterPro IPR002656) family of proteins and also as an acyltransferase_3/putative acetyl-CoA transporter (Transporter Classification Database number TC 9.B.97). As such, $OatA_N$ is thought to span the cytoplasmic membrane and function as an *O*-acyltransferase to shuttle acetyl groups from an unknown source for presentation to the C-terminal extracellular domain ($OatA_C$), which subsequently transfers them onto MurNAc residues (4).

Our earlier structural and biochemical studies of $OatA_C$ from both *S. aureus* (32) and *S. pneumoniae* (33, 34) demonstrated that this domain functions like an SGNH hydrolase in which the C-6 hydroxyl group of muramoyl residues serves as the acceptor for PG O-acetylation instead of water as for a hydrolase. Nothing, however, is known mechanistically nor structurally about the cognate $OatA_N$ or other members of AT-3, and little insight has been gained from studies on any other system translocating acetyl groups across a membrane for their transfer to a glycan. The concept of the two-step coordinated reaction for the overall O-acetylation of extracytoplasmic glycans was first proposed by Higa et al. (35) in their study of a sialyl *O*-acetyltransferase embedded in the Golgi membrane of the rat liver. These early investigators used a chemical modification approach to identify the participation of an essential histidyl and lysyl residues for the first step translocation reaction. More recently, a site-directed mutagenesis of the gene encoding *Salmonella* Typhimurium O-antigen *O*-acetyltransferase A (OafA) confirmed the importance of an Arg-X-X-Arg motif (36) identified previously in this enzyme (37) and a *Shigella flexneri* homolog, Oac (38). The Arg and His residues in an Arg/Lys-X_{10}-His motif were also found to be important for function in OafA, and they are proposed to interact with acetyl-CoA, assuming that this metabolite serves as the acetyl donor for the enzyme (36). Pearson et al. (36) also observed that, while this latter motif is present in all AT-3 homologs, the Arg-X-X-Arg motif together with a Gly-Gly-Phe-(Val/Ile/Leu)-Gly-Val-Asp-(Ile/Val/Leu) motif are found uniquely in AT-3 domains fused to a cognate SGNH domain. In addition to OatA and the O-antigen and *O*-acetyltransferases noted above, members of this subfamily of enzymes are present in other important bacterial pathogens. Examples include OatB and Lot3 that O-acetylate GlcNAc in *Lactobacillus* PG and *N. meningitidis* lipooligosaccharides, respectively. In the intervening years between these studies, little other knowledge has been gained.

Herein, we present a biochemical characterization of the AT-3 domain of OatA. We experimentally determined the topology of *S. aureus* $OatA_N$ (*Sa*$OatA_N$), which we find to differ significantly from that predicted in silico. Using two novel assays (one each in situ and in vitro) coupled with site-specific replacements of consensus amino acids, we identified catalytically essential Arg, His, and Tyr residues. Based on these data, combined with our identification of two acetyl intermediates, we propose a mechanism for the translocation of acetyl groups from cytoplasmic acetyl-CoA to an external loop of *Sa*$OatA_N$ that serves as the acetyl donor for the O-acetylation of PG by $OatA_C$.

Results

OatA Contributes to Lysozyme Resistance. To assess the function of OatA in situ, we developed a phenotypic assay that harnessed lysozyme resistance as the read out. This utilized a mutant of *S. aureus* USA300 we engineered, *S. aureus* USA300 Δ*oatA*, that has a marker-less deletion of *oatA*. *S. aureus* USA300 and *S. aureus* USA300 Δ*oatA* were grown in liquid culture in the presence of increasing concentrations of lysozyme to determine minimal inhibitory concentration (MIC) values for lysozyme. Lysozyme only caused a lag in growth of *S. aureus* USA300 Δ*oatA* and did not result in complete cell death over an 18-h growth period (*SI Appendix*, Fig. S1*A*). It is known that the abolishment of both PG O-acetylation and wall teichoic acid (WTA) production results in increased lysozyme sensitivity compared to the lack of either alone (39). Tunicamycin is a selective and potent inhibitor of TarO, the enzyme that catalyzes the first committed step in WTA synthesis, without causing other significant growth defects in *S. aureus* at low concentrations in rich media (40). We therefore tested lysozyme sensitivity of the two *S. aureus* USA300 strains in the presence of 0.4 μg/mL tunicamycin. Under these conditions, an MIC of 1 mg/mL lysozyme was determined for *S. aureus* USA300 Δ*oatA*, with little effect on the wild-type strain at 4 mg/mL lysozyme (Fig. 1*A* and *SI Appendix*, Fig. S1*B*). Lysozyme resistance was restored to *S. aureus* USA300 Δ*oatA* by complementation *in trans* with His-tagged *Sa*OatA on a constitutive expression plasmid (pACCJ3). Complementation with an empty vector (pALC2073) had no effect.

Lysozyme Resistance Correlates with PG O-Acetylation. To confirm the correlation between the lysozyme sensitivity observed in the functional complementation assay and OatA activity, we determined the PG O-acetylation levels in the two *S. aureus* USA300 strains. The PG O-acetylation level of *S. aureus* USA300 was ~40%, and there was no detectable acetylation in *S. aureus* USA300 Δ*oatA* (Fig. 1*B*). In accordance with the functional complementation assay results, *S. aureus* USA300 Δ*oatA* complemented with pACCJ3 had ~35% PG O-acetylation.

Both *Sa*$OatA_C$ and Full-Length *Sa*OatA Have Esterase Activity In Vitro. The gene encoding full-length *Sa*OatA was cloned with a His_{10}-tag, expressed in *Escherichia coli* C43(DE3), and purified by immobilized metal ion affinity chromatography to apparent homogeneity as determined by sodium dodecyl sulfate–polyacrylamide gel electrophoresis (SDS-PAGE) analysis (*SI Appendix*, Fig. S2*A*). Yields were ~3 mg protein per liter of culture. We also produced and purified *Sa*$OatA_C$ (residues 445 to 601) as previously described (32). As an SGNH hydrolase domain, we recently demonstrated that *Sa*$OatA_C$ functions as a weak esterase, with activity toward the pseudo substrates *p*-nitrophenyl acetate (pNP) and 4-methylumbelliferyl acetate (4MU-Ac), while the variant lacking a catalytic Ser residue was shown to be inactive (32). Consistent with this earlier study, purified *Sa*$OatA_C$ in 5% dimethyl sulfoxide (DMSO) at pH 6.5 had K_M and k_{cat}/K_M values of 112 μM and 42 $M^{-1} \cdot s^{-1}$, respectively, for 4MU-Ac as substrate. We found that full-length *Sa*OatA was also active as an esterase on 4MU-Ac under the same conditions, but its specific activity was only 78% of that of *Sa*$OatA_C$ (*SI Appendix*, Fig. S3). This apparent reduced level of activity of *Sa*OatA likely results from its aggregation when prepared at concentrations required for in vitro studies; evidence for such aggregation was observed with SDS-PAGE analyses (*SI Appendix*, Fig. S2). To determine if *Sa*$OatA_N$ alone can function as an esterase, we generated a recombinant variant of full-length *Sa*OatA lacking a catalytically active *Sa*$OatA_C$ by site-specific replacement of its catalytic nucleophile Ser453 with Ala (*SI Appendix*, Fig. S2*B*). (S453A) *Sa*OatA was indeed active toward 4MU-Ac, but its specific activity was only 69% and 54% of that of full-length *Sa*OatA and *Sa*$OatA_C$, respectively, suggesting that this substrate is not preferred by the AT-3 domain (*SI Appendix*, Fig. S3).

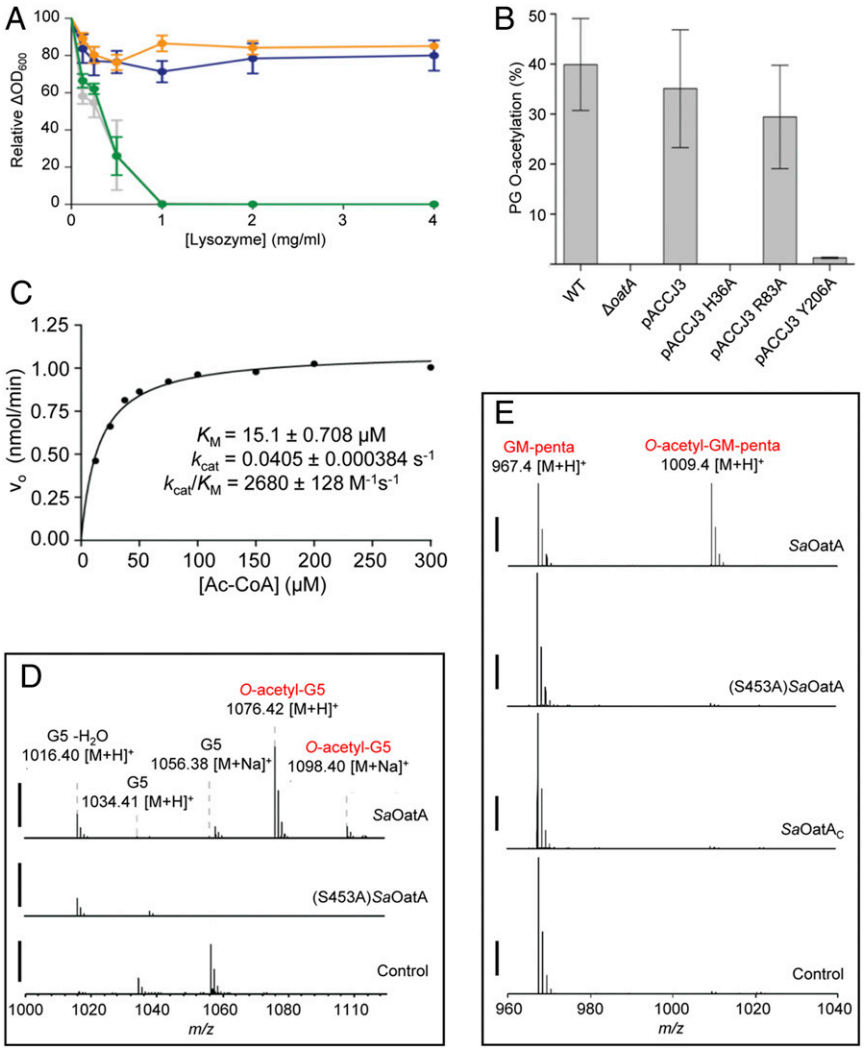

Fig. 1. In situ and in vitro activity of *Sa*OatA. (*A*) Effect of OatA production on lysozyme sensitivity in strains of *S. aureus*. Cultures of *S. aureus* USA300 (blue), *S. aureus* USA300 Δ*oatA* (green), *S. aureus* USA300 Δ*oatA* pACCJ3 (orange), and *S. aureus* USA300 pALC2073 (gray) were incubated for 12 h in the presence of 0.4 μg/mL tunicamycin and lysozyme at the concentrations indicated. Error bars denote SD ($n = 3$). (*B*) PG O-acetylation levels of *S. aureus* USA300 strains. Concentrations of muramic acid and base-labile acetyl groups in purified samples of PG were determined to provide the relative percentage of PG O-acetylation in each strain. Error bars denote SD ($n = 3$). (*C*) Kinetic analysis of *Sa*OatA acting as an esterase with acetyl-CoA as substrate. The steady-state parameters of 5 μM *Sa*OatA were determined in 50 mM sodium phosphate buffer, pH 7.0. "±" denote SD ($n = 3$); error bars are smaller than the height of the symbol. Activity of *Sa*OatA as a PG *O*-acetyltransferase with (*D*) pentaacetyl-chitopentaose (G5) and (*E*) semisynthetic muroglycan oligomers as acceptors. Enzymes (5 μM) in 50 mM sodium phosphate buffer, pH 6.5 were incubated with 1 mM acetyl-CoA and either 1 mM pentaacetyl-chitopentaose or 10 μg/mL semisynthetic muroglycan oligomers (GM-penta) for 18 h prior to QTOF-MS analysis. Control, reaction mixture without added enzyme. The solid bars to the left of the spectrograms presented in *D* and *E* denote 2,500 ion counts.

Only Full-Length *Sa*OatA Uses Acetyl-CoA as a Substrate. To test both full-length *Sa*OatA and *Sa*OatA$_C$ for thioesterase activity against acetyl-CoA, we adapted the chromogenic assay of Grassetti and Murray (41) that monitors the release of CoASH. With *Sa*OatA$_C$, we did not detect any release of CoASH from acetyl-CoA. This is in keeping with the earlier finding that *Sa*OatA$_C$ is unable to O-acetylate pentaacetyl-chitopentaose (G5) when acetyl-CoA is supplied as the acetyl donor (34). However, full-length *Sa*OatA was active toward acetyl-CoA (*SI Appendix*, Fig. S4*A*), indicating that the thioesterase active site is located within *Sa*OatA$_N$. Interestingly, (S453A)*Sa*OatA was weakly active toward acetyl-CoA, retaining only 5.4% specific activity compared to *Sa*OatA. This suggested that, whereas *Sa*OatA$_C$ alone is not active on acetyl-CoA, both domains of *Sa*OatA are required for efficient hydrolysis of this substrate.

We determined the steady-state parameters for full-length *Sa*OatA acting as a thioesterase on acetyl-CoA as substrate (Fig. 1*C*). The determined K_M value of 15 μM was 77- and 6-fold lower than that of *Sa*OatA$_C$ for the pseudo substrates *p*NP-Ac and 4MU-Ac, respectively. Likewise, the overall catalytic efficiency of *Sa*OatA, as reflected by k_{cat}/K_M, was much higher with acetyl-CoA as substrate compared to *Sa*OatA$_C$ acting on these two pseudo substrates.

OatA Utilizes Acetyl-CoA for PG O-Acetylation. The kinetic data presented above suggested that acetyl-CoA may be the natural substrate for the O-acetylation of PG by full-length *Sa*OatA. To test this in vitro, we analyzed full-length *Sa*OatA, *Sa*OatA$_C$, and (S453A)*Sa*OatA independently as *O*-acetyltransferases using our previously established transferase assay (42) with acetyl-CoA as a donor and pentaacetyl-chitopentaose (G5) as a model acceptor. Reaction products were analyzed by liquid chromatography–mass spectrometry (LC-MS) and an acetylated product was only detected in reactions with wild-type, full-length *Sa*OatA; neither *Sa*OatA$_C$ nor (S453A)*Sa*OatA produced acetylated G5 (Fig. 1*D*). Confirmation for the identification of O-acetylated G5 was obtained by tandem MS (MS/MS) analysis (*SI Appendix*, Fig. S4*B*). We also tested *Sa*OatA's ability to acetylate semisynthetically prepared oligomers of GlcNAc-MurNAc-pentapeptide (GM-penta) as a model acceptor for PG (34) using acetyl-CoA as donor. Reaction products were digested with mutanolysin for subsequent LC-MS/MS analysis as described previously (34). As observed with G5, only full-length *Sa*OatA was capable of O-acetylating these muroglycans with acetyl-CoA as the donor (Fig. 1*E*). Combined, these data suggested that acetyltransfer to acceptor glycans requires OatA$_N$ to remove acetyl groups from acetyl-CoA and OatA$_C$ to transfer them onto the muroglycan acceptor substrate.

Topology of *Sa*OatA$_N$. OatA$_N$ is a member of the Acyl_transf_3 (AT-3) Acyltransferases (Pfam PF01757; InterPro IPR002656), a superfamily that includes a wide variety of integral membrane acyltransferases from all forms of life that often acylate saccharides. It has also been identified as an acyltransferase_3/putative

acetyl-CoA transporter (Transporter Classification Database no. TC 9.B.97). Using in silico tools, it is predicted to be an integral membrane domain involving 11 transmembrane segments (TMS), with a large periplasmic loop between TMS3 and TMS4, and a 20-residue linker from TMS11 to the extracytoplasmic C-terminal SGNH *O*-acetyltransferase domain, $OatA_C$ (Fig. 2*A*).

Initially, we attempted to apply the substituted cysteine accessibility method (SCAM) (43) for the experimental determination of *S. aureus* $OatA_N$ topology within the full-length form of the enzyme. This technique was chosen because it allows the topology to be determined on a nontruncated functional protein within its natural host. However, all attempts to label residues expected to be extracytoplasmic (Leu,42, Ile121, Val205, Gln264), including Gly403 within the putative linker sequence between $OatA_N$ and $OatA_C$, failed. Based on these results, we hypothesized that the extracytoplasmic Cys residues were inaccessible to the methoxypolyethylene glycol maleimide (PEGmal)-labeling and 2-(trimethylammonium)ethyl methane thiosulfonate (MTSET)-blocking reagents due to interactions between *Sa*$OatA_N$ and cognate *Sa*$OatA_C$ and/or other membrane proteins.

Due to our lack of success with SCAM, we used the PhoA-LacZα method (44) to determine the topology of $SaOatA_N$. This in situ method involves the generation and expression of chimeras composed of C-terminally truncated forms of the protein of interest with dual reporter enzymes, *E. coli* β-galactosidase LacZα, which is only active in the cytoplasm, and the *E. coli* alkaline phosphatase PhoA, which is only active in the bacterial periplasm. When localized to the periplasm, the PhoA-LacZα reporter will display high alkaline phosphatase activity but no β-galactosidase activity. Conversely, if the dual reporters are localized to the cytoplasm, only high β-galactosidase activity will be detected; detection of both activities indicates localization within the membrane. We generated both a random 3′ gene truncation library of *oatA* from *S. aureus* American Type Culture Collection 6538 fused to *phoA-lacZα*, and targeted truncations were cloned for regions of the protein lacking sufficient coverage in the random truncation library. Based on the data obtained for all 53 truncations, the normalized alkaline phosphatase:β-galactosidase activity ratio (NAR) cutoffs were set at <0.1 and >4.0 for cytoplasmic and extracellular locations, respectively; NAR values of 0.1 to 4.0 denoted transmembrane locations of the truncation. The results for all truncations are given in *SI Appendix*, Table S1, and they were mapped onto the predicted topology map for *Sa*$OatA_N$ (Fig. 2*A*). Whereas these experimental data are consistent with the prediction for the first three transmembrane segments, the data deviate significantly for the rest of the domain.

To develop a topology model that more accurately reflects the experimental evidence, the PhoA-LacZα fusion tagging data were evaluated in context with in silico predictions (*SI Appendix*, Fig. S5*A*), including general rules for transmembrane proteins; ~15 to 20 amino acids are needed for α-helical TMS to cross the

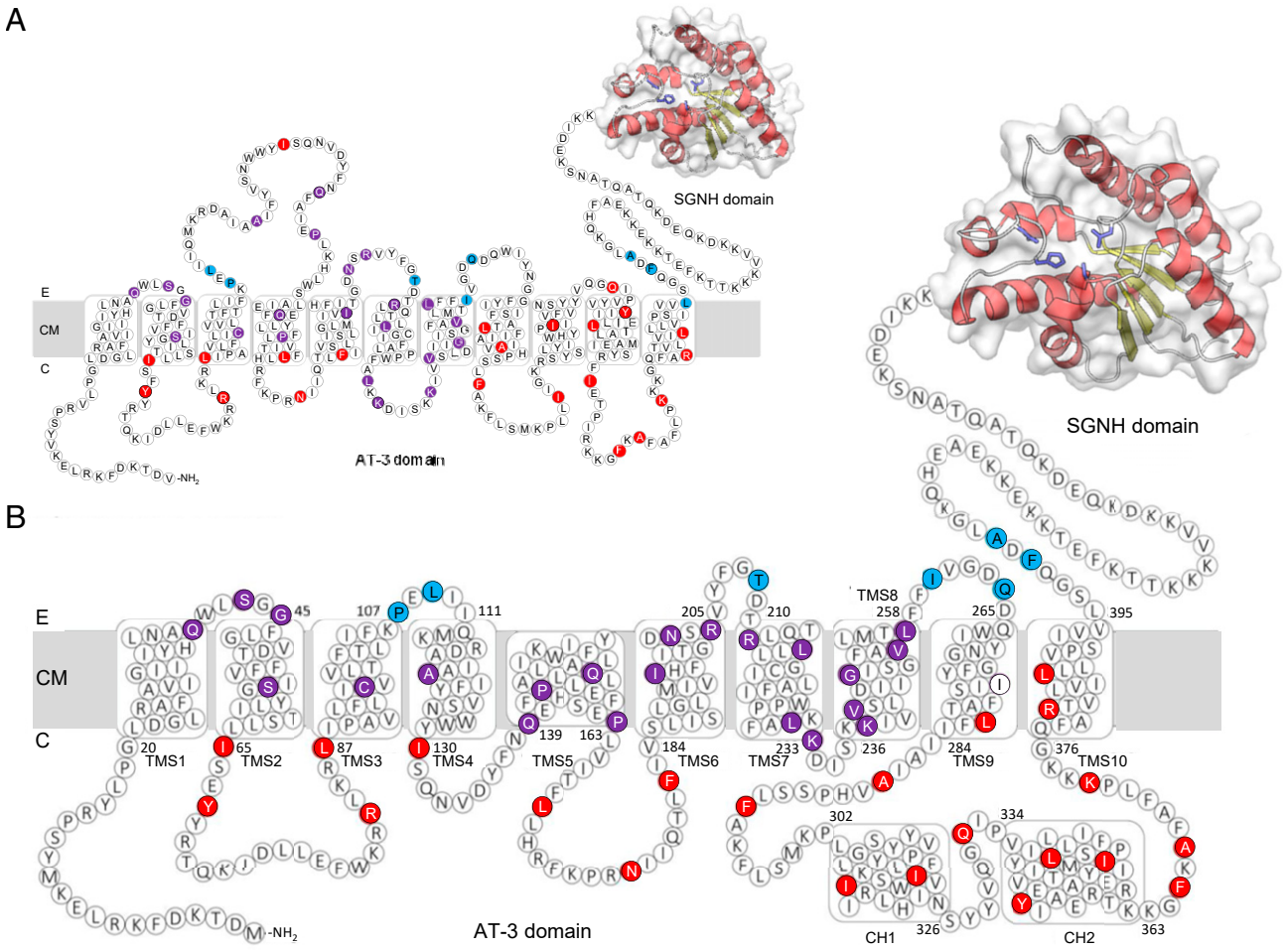

Fig. 2. Topology maps of the AT-N domain of *S. aureus* OatA. (*A*) Consensus in silico prediction of *Sa*$OatA_N$ using TopCons. The PhoA-LacZα fusion data are mapped onto the consensus in silico topology prediction. Each colored residue represents the terminal amino acid of truncation, and the color denotes the location of the truncation: red, cytoplasm; purple, transmembrane; blue, periplasm. (*B*) The adjusted topology model of *Sa*$OatA_N$ to accommodate both the experimental PhoA-LacZα fusion data and in silico predictions of secondary structures. E, external; CM, cytoplasmic membrane; C, cytoplasm.

membrane, and successive positive amino acids are not usually found in a TMS. For large regions of the protein found experimentally to be localized to the same compartment, helix prediction software was used to predict where helices would likely form. The overall result was a new topology model for *Sa*OatA$_N$ with 10 TMS, four extracytoplasmic loops, and four cytoplasmic loops (Fig. 2*B*). Both the C-terminal and N-terminal ends of TMS5 were located in the cytoplasm, suggesting that TMS5 is a membrane-penetrating region, or a re-entrant helix, and not a transmembrane helix. The cytoplasmic loop between TMS8 and TMS9 was the longest, consisting of 92 residues, and it is predicted to form two cytoplasmic helices (CH1 and CH2). Neither CH1 nor CH2 are predicted to be amphipathic, but both are characterized as having alternating hydrophilic and hydrophobic ends (*SI Appendix*, Fig. S5*B*). Thus, the N-terminal end of CH1 and the C-terminal end of CH2 have low mean hydrophobicities ($<H_0>$ = 0.600 and 0.245, respectively), whereas the C-terminal and N-terminal ends of CH1 and CH2, respectively, are much more hydrophobic ($<H_0>$ = 1.023 and 1.204, respectively). This suggests that the C-terminal end of CHI may extend from the cytoplasm to associate with the membrane surface through a small hydrophobic patch, while the N terminus of CH2 associates with the membrane periphery, and its C-terminal end extends back into the cytoplasm.

Identification of Amino Acid Residues Essential for OatA$_N$ Function. ***In situ studies.*** We applied the lysozyme sensitivity assay to identify amino acids essential within *Sa*OatA$_N$ for the function of OatA in situ. A multiple sequence alignment was prepared to identify invariable or highly conserved residues among gram-positive OatA homologs (*SI Appendix*, Fig. S6), and then they were mapped onto our topology map (Fig. 3*A*). Of the 29 invariant and 49 highly conserved residues identified, several appear to be clustered in or near TMS1 and TMS2 as well as TMS5 and cytoplasmic helices 10 and 11. These include the Arg-X-X-Arg and Arg/Lys-X$_{10}$-His motifs identified in earlier studies of other AT-3 domains that are associated with cognate SGNH domains like OatA (36–38). We replaced 23 targeted residues with Ala by site-directed mutagenesis of the *oatA* gene in pACCJ3, and the resulting plasmids were used to complement *S. aureus* USA300 Δ*oatA*. Both this latter strain transformed with empty vector and *S. aureus* USA300 Δ*oatA* pACCJ3 (*viz.* transformed with wild-type OatA) were used as controls. The growth of each complemented strain in the presence of 0.4 μg/mL tunicamycin and increasing concentrations of lysozyme was monitored to assess the effect of the respective amino acid replacements on lysozyme sensitivity as a measure of function. Whereas *S. aureus* USA300 Δ*oatA* complemented with wild-type *oatA* had full lysozyme resistance at the highest concentration tested (4 mg/mL), single amino acid substitutions caused significant lysozyme sensitivity for 10 of the conserved residues (Arg25, His36, Phe52, Arg86, Tyr136, Trp149, Glu154, Tyr206, Tyr311, and Glu357), while we found moderate lysozyme sensitivity for four others (Ser56, Arg83, Asn126, and Tyr314) (Fig. 3*B*).

To ensure that the 14 functionally impaired *Sa*OatA variants were expressed and localized correctly, the membranes from each *S. aureus* USA300 Δ*oatA*-complemented strain were isolated and probed for *Sa*OatA presence by anti-His Western analysis. Each *Sa*OatA variant was found in the membrane in approximately equal amounts, suggesting that the observed lack of function was not due to insufficient expression or improper membrane insertion of the OatA variants (Fig. 3 *A*, *Inset*). Confirmation of the correlation between lysozyme sensitivity and OatA function was again obtained by analyzing the PG from representative mutants for O-acetylation. The PG purified from the mutants producing single amino acid variants (H36A)*Sa*OatA and (Y206A)*Sa*OatA and displaying full lysozyme sensitivity had 0 and 1.3% O-acetylation, respectively, while the strain producing (R83A)*Sa*OatA and displaying only partial lysozyme sensitivity had ~29% PG O-acetylation (Fig. 1*B*).

We investigated the importance of charge or functional groups associated with some of these residues on activity by replacing them with alternate amino acids. The replacement of Arg25 and Arg86 individually with Lys had no effect on lysozyme resistance, suggesting that the positive charge of Lys can compensate for that of Arg at these positions (Fig. 3*B*). We found that neither Asp nor Gln could compensate for the functional role of Glu154, but partial activity was retained with the replacement of Glu357 with Asp. As with Glu154, we found both Tyr136 and Tyr206 to be essential residues; their replacement with either Phe or Ser resulted in mutant strains sensitive to lysozyme. However, the mutant producing (Y311S)*Sa*OatA retained wild-type levels of lysozyme resistance.

In vitro studies. We subcloned and expressed a selection of the mutated *oatA* genes in *E. coli*, and the recombinant *Sa*OatA variants were purified to apparent homogeneity in the same manner as for *Sa*OatA and (S453A)*Sa*OatA (*SI Appendix*, Fig. S2). We tested each for esterase and transferase capacity by incubating them with acetyl-CoA alone (esterase) and together with pentaacetyl-chitopentaose (G5) as a pseudoacceptor (transferase). For the latter, we assayed for G5 O-acetylation by LC-MS/MS. The (R25A), (R86A), and (E154A)*Sa*OatA variants retained 18.4%, 22.1%, and 4.76% esterase activity, respectively (Fig. 3*C*), with low amounts of O-acetylated G5 detected by LC-MS (*SI Appendix*, Fig. S7). (H36A)*Sa*OatA retained only 0.64% apparent esterase activity and no transferase activity was detected. The (Y206A)*Sa*OatA variant was devoid of both esterase and transferase activity. Interestingly, (Y136A)*Sa*OatA displayed 155% esterase activity toward acetyl-CoA; however, no acetylated G5 was detected by LC-MS in the transferase assay, suggesting that this residue does not contribute directly to the catalytic mechanism of *Sa*OatA$_N$. (R25K)*Sa*OatA also displayed increased esterase activity compared to wild-type (178%); however, this variant was functional as an *O*-acetyltransferase.

We determined the steady-state kinetic parameters for the (Y136A) and (R25K)*Sa*OatA variants as esterases (Fig. 3*D*). The K_M of (R25K)*Sa*OatA for acetyl-CoA was almost double that of wild-type OatA. However, the V_{max} was also double, such that the overall efficiency of the enzyme, as reflected by k_{cat}/K_M, was only slightly increased compared to wild-type. Due to limitations of the assay, we could not saturate (Y136A)*Sa*OatA with acetyl-CoA, but extrapolation of the data suggests a significantly increased K_M of 133 μM and decreased k_{cat}/K_M of 1,170 $M^{-1} \cdot s^{-1}$.

Trapping *O*-Acetyl-Enzyme Intermediates. Previously, we demonstrated the accumulation of an acetyl intermediate within *Sa*OatA$_C$ involving its catalytic nucleophile Ser453 by a real-time analysis of its reaction with *p*NP-Ac as an acetyl donor (32). Recognizing that *Sa*OatA appears to have two catalytic centers, we postulated that a residue within *Sa*OatA$_N$ may become acetylated in the translocation/transferase mechanism and that this residue may serve as the acetyl donor for *Sa*OatA$_C$. Thus, we attempted to repeat the trapping experiment using full-length *Sa*OatA in the presence of acetyl-CoA. However, being a large integral membrane protein, we experienced solubility issues during the chromatography step of the LC-MS analysis. We found that we could (barely) detect native, untreated *Sa*OatA with a deconvoluted mass of 70,871.6 Da, the expected mass for the unbound protein, but only when a low concentration (4.3 mg/mL; 60 μM) sample was analyzed. However, when injected in the presence of acetyl-CoA, a suppression of the already low-intensity multiply charged *Sa*OatA ions was observed and precluded spectral deconvolution to monoisotopic mass species. This included the loss of the monoisotopic mass peak at 70,871.6 that corresponded to unmodified *Sa*OatA, suggesting that acetylated species were nonetheless produced. We suspected that, unlike the situation with OatA$_C$ with its single active center, full-length OatA possesses at least two which may give rise to a mixed population of ionic species with different extents of acetylation, compounded by the potential of additional sodium adducts.

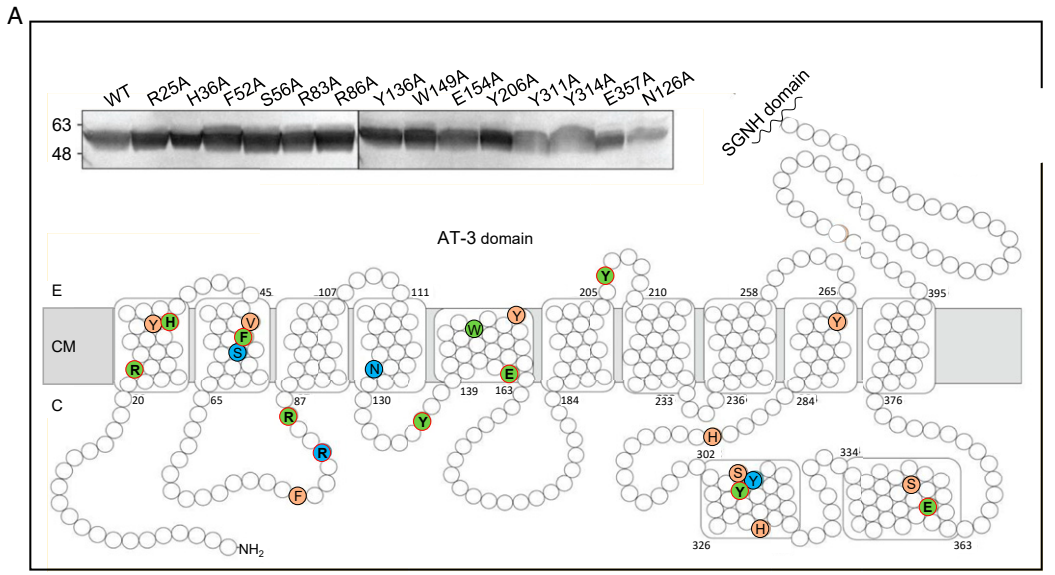

B

Variant	MIC (mg/mL)[1]
Δ*oatA*	1
WT (pACCJ3)	> 4
R25A	0.5
R25K	> 4
Y35A	> 4
H36A	0.5
V49A	> 4
F52A	0.5
S56A	4
F79A	> 4
R83A	4
R86A	0.25
R86K	> 4
N126A	2
Y136A	0.25
Y136F	0.25
Y136S	0.25
W149A	1
E154A	0.5
E154D	0.5
E154Q	0.5
Y158A	> 4
Y206A	0.5
Y206F	1
Y206S	0.5
Y269A	> 4
H289A	> 4
S310A	> 4
Y311A	0.5
Y311F	0.5
Y311S	> 4
Y314A	4
H317A	> 4
S352A	> 4
E357A	0.5
E357D	1-2
E357Q	0.25

C

Enzyme Variant	Esterase Activity		Transferase Activity
	Specific Activity (nmol•min^{-1}•mg^{-1})	Relative Activity (%)	
WT	28.8 ± 0.20	100	yes
R25A	5.28 ± 0.07	18.4	yes
R25K	51.3 ± 0.23	178	yes
H36A	0.18 ± 0.05	0.64	no
R86A	6.37 ± 0.02	22.1	yes
Y136A	44.6 ± 0.48	155	no
E154A	1.37 ± 0.05	4.76	yes
Y206A	N.D.	0	no
S453A	-	5.40	no

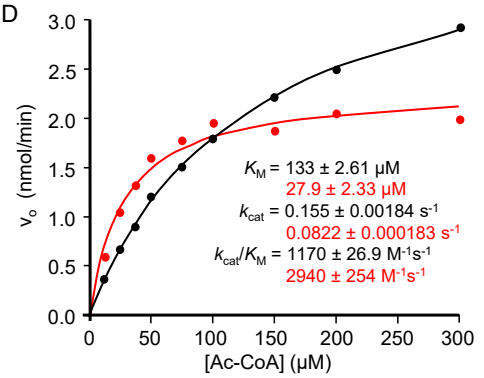

Fig. 3. Identification of conserved and functional residues in *Sa*OatA$_N$. (*A*) Invariable and highly conserved residues were identified by bioinformatic analysis of OatA homologs and mapped onto the topology map of *Sa*OatA$_N$. Selected residues were individually replaced with Ala, and the resultant *Sa*OatA variants were assessed for their ability to provide lysozyme resistance in a Δ*oatA* background of *S. aureus* USA300. The amino acid color denotes the functional complementation assay result: completely lysozyme sensitive (green), partially lysozyme sensitive (blue), or completely lysozyme resistant (orange). E, external; CM, cytoplasmic membrane; C, cytoplasm. Residues identified as important for substrate-binding and the catalytic mechanism are outlined in red. (*Top*) The membranes from lysozyme-sensitive *S. aureus* USA300 Δ*oatA*-complemented strains (bolded variants listed in *B*) were isolated and probed for *Sa*OatA by anti-His Western blotting to ensure proper expression and membrane localization. Molecular weight markers (kDa) are shown on *Left*. (*B*) In situ activity of *S. aureus* USA300 Δ*oatA* expressing single amino acid variants of *Sa*OatA as monitored by their sensitivity to lysozyme. The MIC values of lysozyme were determined by culturing *S. aureus* USA300 Δ*oatA* expressing *oatA* in trans in the presence of 0.4 μg/mL tunicamycin and increasing concentrations of lysozyme (0 to 4 mg/mL). Each variant was tested in technical and biological triplicates. (*C*) Esterase and transferase activities of *Sa*OatA variants with acetyl-CoA as acetyl donor. Reactions were conducted in 50 mM sodium phosphate buffer, pH 7.0, containing 5% (vol/vol) DMSO at 25 °C with 0.1 mM acetyl-CoA and 0.2 mM DTDP (5% ethanol replaced DMSO for reactions with S453A). Transferase assays included 1 mM pentaacetyl-chitopentaose (G5) as an acceptor, and products were detected by LC-MS as described in the legend to Fig. 1*E*. "±" denotes SD; N.D. = no detectable activity. (*D*) Determination of the steady-state parameters of (Y136A)*Sa*OatA (black) and (R25A)*Sa*OatA (red) acting as esterases on acetyl-CoA. The reaction conditions for these determinations are described in the legend to Fig. 1*C*.

We encountered similar obstacles with the matrix-assisted laser desorption ionization time-of-flight (MALDI-TOF) MS analysis of *Sa*OatA and its possible adducts. Despite the amount of protein applied to the chips, we detected very weak signals (*SI Appendix*, Fig. S8). Moreover, as with the MALDI-TOF MS analyses of other membrane proteins (e.g., ref. 45), the signals were very broad, and their center of mass was shifted over 4,000 Da from the expected mass of the protein. This shift has been attributed to the presence of protein-bound lipids and/or detergents. However, despite the breadth of the signals, we observed a difference between the average *m/z* ratios of *Sa*OatA in the absence and presence of acetyl-CoA of 124.9 Da, the approximate mass of three acetyl groups (expected mass, 126.03 Da).

Despite our failure to detect modified *Sa*OatA directly by intact protein LC-MS but encouraged by the MALDI-TOF MS data, we attempted to identify site(s) of acetylation within a protease digest of full-length *Sa*OatA. LC–quadrupole-TOF MS/MS analysis of the peptides from a control digestion of untreated *Sa*OatA provided 56% coverage of the native *Sa*OatA sequence; not surprisingly, there was minimal coverage of the N-terminal membrane-spanning helices (46–48). Searching for peptides modified by acetyl groups (*viz.* +42.01 Da) using the Peaks XPro software, we detected the nonspecific acetylation of His557 and Tyr581, albeit with low confidence and high mass error. These two residues are surface exposed on separate faces of *Sa*OatA$_C$, and their side-chain O atoms are located 24.3 and 18.8 Å from the catalytic Ser453 side-chain oxygen, respectively; presumably, they became nonspecifically acetylated in the *E. coli* expression host. A similar treatment and analysis of a protease digest of *Sa*OatA pre-incubated with acetyl-CoA yielded a slightly better coverage of

60%, and again, we observed nonspecific acetylation of Tyr581 together with another surface-exposed residue Tyr490, also located in *Sa*OatA$_C$ and 28.4 Å from the active site. The only unique acetylated peptide species, which could be detected in multiple scans of both datasets with high confidence and low mass error and confirmed by subsequent MS/MS fragmentation analysis, mapped to catalytic Ser453 of *Sa*OatA$_C$ (*SI Appendix*, Fig. S9). This was expected given this acetyl intermediate had been identified previously in our earlier study with isolated *Sa*OatA$_C$ (32). Nonetheless, this confirmed that while the isolated domain alone is unable to utilize acetyl-CoA as an acetyl donor, acetyl groups from this natural metabolite are provided directly to it through *Sa*OatA$_N$ for PG O-acetylation. Interestingly, we also observed the Ser453-Lys464 peptide with a moderate score of acetylation in the digest of the untreated control preparation of *Sa*OatA. Presumably, this acetylation occurred by the enzyme's acquisition of acetyl from acetyl-CoA pools in the cytoplasm of the *E. coli* expression host.

Recognizing that the specific activity of (S453A)*Sa*OatA as a thioesterase is significantly lower than that of the wild-type enzyme, we postulated that we may be able to trap any acetyl-product of the N-terminal acyltransferase domain within this enzyme variant. LC-MS/MS analysis of a protease digest of (S453A)*Sa*OatA pretreated with acetyl-CoA provided 65% coverage of the protein. As with the other analyses, we detected low levels of nonspecific acetylations of Tyr574 and Tyr581 and additionally His557, which all mapped to our structure of OatA$_C$ as surface-exposed residues distant from the catalytic center. However, we also observed with high confidence and in multiple scans the unique acetylated peptides Val205–Lys232 and Val205-Lys233 containing the essential Tyr residue, Tyr206. The precursor ion was reliably matched to the OatA sequence, and the mass shift of 42.01 Da of Tyr206 was confirmed by MS/MS fragmentation with high confidence and low mass error, indicating its acetylation (*SI Appendix*, Fig. S9). This finding is consistent with essential Tyr206 serving as the catalytic nucleophile for the acquisition of acetyl groups from acetyl-CoA.

***O*-Acetyl-Tyr Is a Substrate for OatA$_C$.** The data presented above indicated the presence of two active sites within *Sa*OatA, involving Tyr206 and Ser453 as the catalytic nucleophiles within *Sa*OatA$_N$ and *Sa*OatA$_C$, respectively. Being located on a small extracellular loop linking transmembrane segments, we postulated that Tyr206

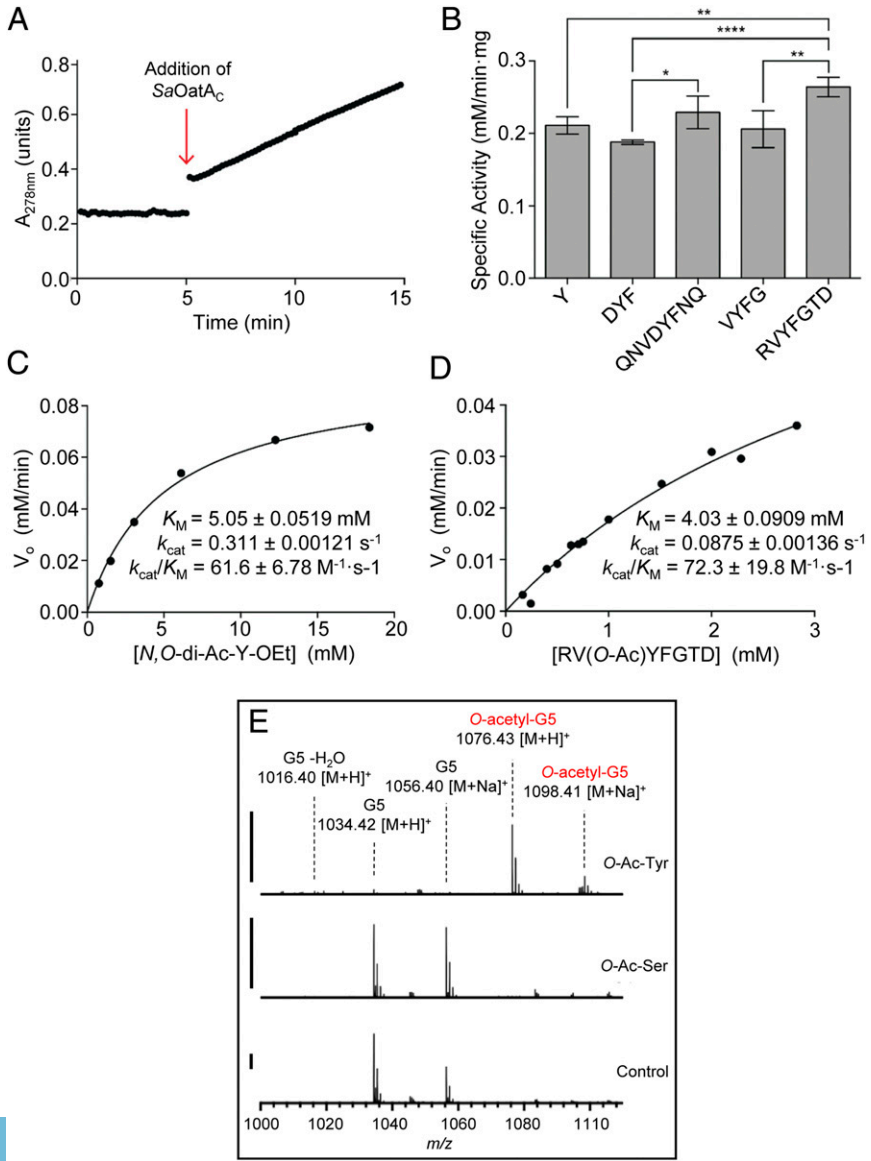

Fig. 4. Esterase and O-acetyltransferase activity of OatA$_C$ with O-acetyl-Tyr peptides as acetyl donor. (*A*) Representative assay for determination of esterase activity. The absorbance of acetylated peptide in 50 mM sodium phosphate pH 6.5 and DMSO was monitored at 278 nm for spontaneous hydrolysis of the acetyl group. *Sa*OatA$_C$ (5 μM) was then added to the reaction (indicated by red arrow), and the rate of esterase activity was monitored. (*B*) Determination of the specific activity of 5 μM *Sa*OatA$_C$ for each *O*-acetylated peptide at 1 mM in 50 mM sodium phosphate pH 6.5 containing 35% (vol/vol) DMSO. Error bars denote SD ($n = 3$). *$P \leq 0.05$; **$P \leq 0.01$; ****$P \leq 0.0001$. (*C* and *D*) The steady-state parameters were determined for 5 μM *Sa*OatA$_C$ in 50 mM sodium phosphate pH 6.5 and 44% (vol/vol) DMSO using (*C*) 0.76 to 18.4 mM *O*-Ac-Tyr-ethyl ester or (*D*) 0.24 to 2.8 mM Arg-Val-(O-Ac)-Tyr-Phe-Gly-Thr-Asp-amide as substrate. (*E*) LC-MS analysis of reaction products following 18 h incubation of 5 μM *Sa*OatA$_C$ in phosphate buffer containing 4% DMSO with 1 mM G5 as a glycan acceptor and 1 mM of either *O*-acetyl-Tyr-ethyl ester or *O*-acetyl-Ser as an acetyl donor. The solid bars to the left of the spectrograms denote 5,000 ion counts.

also functions to directly transfer acetyl groups between the two catalytic domains and serves as the acetyl donor for *Sa*OatA$_C$. To test this, we prepared as potential substrates synthetic peptides based on the Tyr206 extracellular loop that were O-acetylated at the Tyr hydroxyl group. Given the poor solubility of these acetylated peptides, we needed to conduct the assays in the maximal permissible DMSO concentration. To determine this, we tested the activity of *Sa*OatA$_C$ toward 4MU-Ac in increasing DMSO concentrations up to 60% (*SI Appendix*, Fig. 10*A*). To our surprise, we found that esterase activity peaked at 40% DMSO. It would appear that DMSO helps to stabilize the activity of the *Sa*OatA$_C$ in the same manner as has been observed with other PG metabolizing enzymes, such as the high MW PBPs and SEDS proteins, which are active in vitro only in the presence of 20 to 30% DMSO (e.g., ref. 49). In 35% DMSO, the K_M of *Sa*OatA$_C$ for 4MU-Ac was similar to that in 5% DMSO, but its k_{cat} was significantly higher, resulting in an overall efficiency of the enzyme that was sixfold greater under these conditions (*SI Appendix*, Fig. S10 *B* and *C*).

We prepared *N*-acetyl-Val-(*O*-acetyl)-Tyr-Phe-amide (VYF), *N*-acetyl-Val-(*O*-acetyl)-Tyr-Phe-Gly-amide (VYFG), and *N*-acetyl-Arg-Val-(*O*-acetyl)-Tyr-Phe-Thr-Asp-amide (RVYFGTD) as representative short and long peptides, respectively, of the Tyr206 extracytoplasmic loop. Unfortunately, the extremely low solubility of VYF prevented its use for activity assays. *N*-acetyl-Asp-(*O*-acetyl)-Tyr-Phe-amide (DYF) and *N*-acetyl-Gln-Asn-Val-Asp-(*O*-acetyl)-Tyr-Phe-Asn-Gln-amide (QNVDYFNQ) were also prepared as representatives of a cytoplasmic loop in *Sa*OatA (residues 130 to 139). To determine activity, we developed a spectrophotometric assay that monitors the resulting increase in absorbance at 278 nm with the removal of the acetyl group from the Tyr residue of the donor peptide (Fig. 4*A*); the acetylation of Tyr residues suppresses absorbance at 278 nm (50). Unfortunately, substrate availability and solubility, even in 35% DMSO, limited the scope of analyses, and it was only possible to obtain a specific activity with some peptides. For this reason, the O-acetylated peptides were tested in 44% DMSO to maximize substrate solubility while maintaining enzyme activity.

O-acetyl-Tyr-ethyl ester and each of the peptides containing *O*-acetyl-Tyr served as substrates for *Sa*OatA$_C$ acting as an esterase (Fig. 4*B*). Whereas the range of determined specific activities for each of these peptides was small, that for the peptide RVYFGTD was the highest. This peptide alone is predicted to form a loop, which would likely be stabilized by a salt bridge between Arg204 and Asp210, a feature consistent with its position in our topology map of *Sa*OatA$_N$. *Sa*OatA$_C$ was less active toward the internal tetrapeptide of this loop, VYFG, and both DYF and QNVDYFNQ, peptides that comprise in an intracellular loop linking TMS4 to TMS5. We determined the Michaelis–Menten parameters of *Sa*OatA$_C$ for *N,O*-di-acetyl-Tyr-ethyl ester and RVYFGTD (Fig. 4 *C* and *D*), and whereas the K_M values were relatively high, the overall catalytic efficiency of the enzyme for these O-acetylated peptides was nearly double that for the simple pseudo substrate 4MU-Ac (*SI Appendix*, Fig. S10).

Finally, we found that *O*-acetyl-Tyr-ethyl ester, but not *O*-acetyl-Ser, may function as a donor substrate for the O-acetylation of G5 by *Sa*OatA$_C$. The enzyme was incubated with 1 mM of each potential donor substrate and 1 mM G5 as an acceptor for 2 h, and reaction products were analyzed by LC-MS. O-Acetylated G5 was detected only after a reaction with *O*-acetyl-Tyr-ethyl ester (Fig. 4*E*) as a donor.

Discussion

Membrane proteins are notoriously difficult to study due to their poor solubility and low stability in vitro. As such, structural and biochemical information for many membrane-bound enzymes is very limited. This applies to the wide variety of acetyltransferases responsible for the O-acetylation of extracellular glycans, including OatA and all other AT-3 family proteins. The extracytoplasmic C-terminal SGNH hydrolase domain of OatA has been well characterized as a PG *O*-acetyltransferase (32–34), but nothing was known previously about the cognate N-terminal domain beyond homology-based predictions. In this study, we experimentally determined the topology and function of *Sa*OatA$_N$ and provide molecular insights of the acetyl translocation process of any membrane-bound enzyme catalyzing extracytoplasmic O-acetylations of glycans.

The topology map of *Sa*OatA$_N$ generated by PhoA-LacZα fusion mapping enabled a two-dimensional model to be generated (Fig. 2*B*), which differed significantly from that determined using the same method for another AT-3 family protein, Oac, an *O*-acetyltransferase responsible for the O-acetylation of O-antigen in *S. flexneri* (38). However, only 16 truncations of Oac were assayed, and certain regions of the protein were not mapped at all (38), which may account for discrepancies between the Oac and *Sa*OatA$_N$ experimental models. Indeed, our study of 53 truncations of *Sa*OatA$_N$ revealed several unanticipated structural features. Whereas each approach has its limitations, experimental mapping methods have their advantage over in silico predictions which have rigid criteria. Predictions assume each TMS crosses the membrane, and they do not account for certain structural features commonly found in integral membrane proteins, such as peripheral membrane, re-entrant, or partial helices. Each of these elements appears to be present in *Sa*OatA$_N$ including the re-entrant helix TMS5. Our interpretation that TMS5 is a re-entrant helix is based on finding both Ile130 and Leu168 to be located in the cytoplasm. As a typical transmembrane helix has an average length of 25 residues (51), it is unlikely the intervening 38 amino acid residues would form two transmembrane helices. Furthermore, helix prediction software predicts one helix in this region encompassing residues Leu145 to Arg171. We set the bounds of TMS5 by Gln139 and Pro163 because both were located to the membrane, but it is not possible to ascertain whether TMS5 is one long or two short helices based solely on the data obtained. While not being predicted, re-entrant helices are observed in transmembrane proteins with solved structures. For example, *E. coli* undecaprenyl pyrophosphate phosphatase possesses two short adjacent re-entrant helices (52, 53), and the ClC chloride channel from the same bacterium is characterized by six re-entrant regions (54).

The region between TMS9 and TMS10 involving two predicted α-helices was located to the cytoplasm by 11 truncations (Fig. 2*B*). Although these helices are not predicted to be amphipathic, both CH1 and CH2 have large hydrophobic dipole moments over their lengths, suggesting peripheral association with the membrane through their C- and N-terminal ends, respectively (*SI Appendix*, Fig. 5*B*). Peripheral membrane helices are also a common occurrence in membrane proteins. A recently discovered example is with *Streptococcus thermophilus* DltB, a member of the membrane-bound *O*-acyltransferase (MBOAT) family of proteins involved in the D-alanylation of WTAs. The structural model for this protein solved by X-ray crystallography (55) presents several short peripheral membrane helices that contain important functional residues, features that are not predicted in silico. These examples demonstrate the limitations of in silico tools and highlight the value of experimental approaches to determining the structure and topology of membrane proteins.

Our ability to assay *Sa*OatA in vitro permitted us to identify acetyl-CoA as its preferred acetyl donor for PG O-acetylation (Fig. 1). The kinetic parameters we established for this reaction are consistent with acetyl-CoA being its natural substrate. This is supported by our identification of three Arg residues on the cytoplasmic face of *Sa*OatA$_N$ that likely function to coordinate the phosphoryl groups of coenzyme A for its productive binding. These three Arg residues comprise the Arg-X-X-Arg and Arg/Lys-X$_{10}$-His motifs identified earlier in the Oac homologs by others (36–38). The results of our in situ assay (Fig. 3*B*) coupled with the in vitro kinetic analyses of some of the recombinant *Sa*OatA variants confirmed the importance of Arg86 and, to a lesser extent, Arg83 of the

Arg-X-X-Arg motif and both Arg25 and His36 of the Arg/Lys-X_{10}-His motif. Concerning the latter motif, the (R25K)*Sa*OatA variant was generally more active in vitro as a thioesterase, indicating that the retention of positive-charge character is important for function. However, its K_M for acetyl-CoA was approximately twofold higher than that for the wild-type enzyme, strongly supporting the notion that Arg25 and its counterparts in other AT-3 acetyltransferases contributes to acetyl-CoA–binding (36–38). On the other hand, the Arg residues of the Arg-X-X-Arg motif have been proposed to be critical for the assembly of *S. flexneri* Oac (38), but we found no differences in the in situ expression of the (R83A) and (R86A) *Sa*OatA variants (Fig. 3 *A*, *Inset*) suggesting otherwise. Unlike the earlier models for AT-3 topology in which the Arg-X-X-Arg motif is predicted to comprise TMS3, we located both Arg83 and Arg86 on a cytoplasmic loop between TMS2 and TMS3. This positioning is consistent with the rule that positively charged amino acids are usually found in cytoplasmic loops of transmembrane proteins. Moreover, comprising a loop would provide flexibility for the clustering of Arg83 and Arg86 near the cytoplasmic face of TMS1, the location of Arg25, and thereby form an appropriate binding site to accommodate and stabilize the three phosphoryl groups of coenzyme A (Fig. 5*A*). This hypothesis is supported by structural evidence obtained in the examination of acetyl-CoA interactions with other acetyltransferases, such as *N. meningitidis* polysialic acid *O*-acetyltransferase OatWY (56) and *E. coli* galactoside acetyltransferase (57), in which a set of electrostatic interactions involving three Arg/His/Lys residues directly stabilizes these phosphate groups.

Other typical features of binding sites for acetyl-CoA in acetyltransferases include a stacking interaction between an aromatic amino acid residue (often Tyr) and the adenine ring of coenzyme A and the stabilization of the phosphopantothenyl arm of CoA by both polar and nonpolar interactions with the side chains of residue(s) as observed with, for example, *N. meningitidis* OatWY (56). Based on their observed locations, importance for function, and flexibility (or lack thereof) for replacement, we postulate that invariant residues Phe52, Tyr311, Glu357, and possibly Tyr136 contribute to these functions (Fig. 5*A*). Instead of comprising integral membrane segments as initially predicted, Tyr311 and Glu357 are located within the cytoplasm. Tyr311 could be replaced with Ser, but not Ala nor Phe, for the retention of in situ activity, suggesting the requirement for hydrogen bonding capacity. Similarly, Glu357 could be replaced with Asp, but neither Gln nor Ala, indicating the need for anionic character at its position. These characteristics are consistent with these two residues contributing to and stabilizing the binding site for coenzyme A at the cytoplasmic face of the membrane. Phe52, on the other hand, was predicted and observed to be located within the middle of TMS2. This is an appropriate position for hydrophobic interactions with the phosphopantothenyl arm of CoA if the acetylated coenzyme extends up from the cytoplasm within a channel of the protein formed by TMS1, TMS2, and others to present the acetyl group toward the extracytoplasmic face of the protein (Fig. 5*A*). Such an orientation of the acetyl donor would be expected for the translocation of the acetyl group to Tyr206 on the extracellular surface of the protein to serve as substrate for $SaOatA_C$ and eventual transfer to PG. The importance of invariant Phe52 is underscored by it comprising a conserved sequence motif, VxxFFx(I/V/L)SG(F/WY), that was first identified in several O-antigen *O*-acetyltransferases (38, 58).

The functional role of Tyr136 is less clear. This invariant residue was initially predicted to comprise a large extracytoplasmic loop, but our topology mapping located it within a short cytoplasmic loop linking TMS4 to the re-entrant helix TMS5. This residue could not be replaced with either Ala, Ser, or Phe without the impairment of in situ activity, and the K_M of the (Y136A)SaOatA variant for acetyl-CoA was an order of magnitude higher than that of the wild-type enzyme, while their respective k_{cat} values were similar. These features are consistent with a substrate-binding role for Tyr136, and it is conceivable that, like Arg83 and Arg86, its location on a cytoplasmic loop provides its opportunity to comprise the acetyl-CoA–binding site at the cytoplasmic face of the protein (Fig. 5*A*). On the other hand, while lacking transferase activity, (Y136A)SaOatA is more active as an esterase, indicating that Tyr136 in some way contributes to the appropriate positioning of Tyr206 for the effective transfer of acetyl groups between $SaOatA_N$ and $SaOatA_C$. With our understanding of typical integral membrane proteins, these two direct functions involving both cytoplasmic and extracellular events would seem to be mutually exclusive. However, a number of the $SaOatA_N$ transmembrane helices are predicted to be either re-entrant or oblique (*SI Appendix*, Fig. S5*A*), while others were observed to be cytoplasmic. These features are consistent with the overall conformation of the enzyme to be similar to that of the MBOAT family member, D-alanyl carrier protein (DltB). DltB contains a ring of 11 peripheral transmembrane helices, which form an intracellular concave surface and an extracellular structural funnel that extends into the middle of the lipid bilayer of the cytoplasmic membrane and surrounds a central thin structural core (55). The active site located within the central core catalyzes the translocation of D-alanyl residues across the cytoplasmic membrane of gram-positive bacteria for their addition to teichoic acids. It is conceivable that this unique structure may represent a new paradigm for other families of membrane-associated acyltransferases, such as the AT-3 proteins. If so, then it may be possible for a residue such as Tyr136 in *Sa*OatA to serve the two roles of contributing to acetyl-CoA–binding and structurally aligning the catalytic center. Of course, the delineation of Tyr136's role in the function of $SaOatA_N$, and those of the other invariant residues discussed above, awaits structural information at the atomic level.

We identified invariant His36 within TMS1 as being essential for *Sa*OatA activity both in vitro and in situ. Its equivalent has been recognized as being important in many other membrane-bound acetyltransferases, including AT-3 proteins (36). Being 10 residues apart, His36 and Arg25 would be positioned on the same face of TMS1 and separated by a distance of ~16.5 Å, the approximate length of the phosphopantothenyl arm of coenzyme A (Fig. 5*A*). Also recognizing this, Pearson et al. (32) postulated that homologous residues Arg14 and His25 in *S.* Typhimurium OafA provide a potential interaction site for acetyl-CoA. Our finding that (H36A)*Sa*OatA retains only 0.6% residual activity as an esterase compared to wild-type *Sa*OatA and lacks the ability to catalyze acetyl transfer to glycan acceptors suggests an important catalytic role for the residue in the enzyme's mechanism of action. Invariant Glu154 of the re-entrant TMS5 was also determined to be important for catalytic activity. Its replacement with Ala, Asp, or Gln generated weakly active forms of *Sa*OatA, also suggesting a mechanistic role for this acidic residue. If Tyr136 does interact with the adenine ring of coenzyme A, TMS5 would have to be associated with TMS1 and TMS2 and thereby position Glu154 in close proximity to His36.

Considering all of the findings discussed above, we hypothesize that Tyr206, His36, and Glu154 of $SaOatA_N$ form a catalytic triad for the translocation of acetyl groups from the cytoplasm to the extracellular surface of *Sa*OatA (Fig. 5*B* and *SI Appendix*, Fig. S11), which would function in a manner analogous to the catalytic Ser, His, Asp catalytic triad of $OatA_C$ (32–34). Thus, we propose that Glu154 forms a salt bridge with His36, enabling His36 to function as a base to deprotonate Tyr206. Rendered nucleophilic, Tyr206 would attack the thioester carbonyl carbon of acetyl-CoA generating a tetrahedral transition state, which then collapses into a covalently bound acetyl-enzyme intermediate. In this study, Tyr206 was identified as the site of acetylation (*SI Appendix*, Fig. S9), and kinetic studies with model peptides support the notion that *O*-acetyl-Tyr206 serves as the acetyl donor for $SaOatA_C$. It is theoretically possible that His36 functions as the nucleophile to directly attack the carbonyl of the acetyl-CoA thioester to form an initial covalent

MICROBIOLOGY

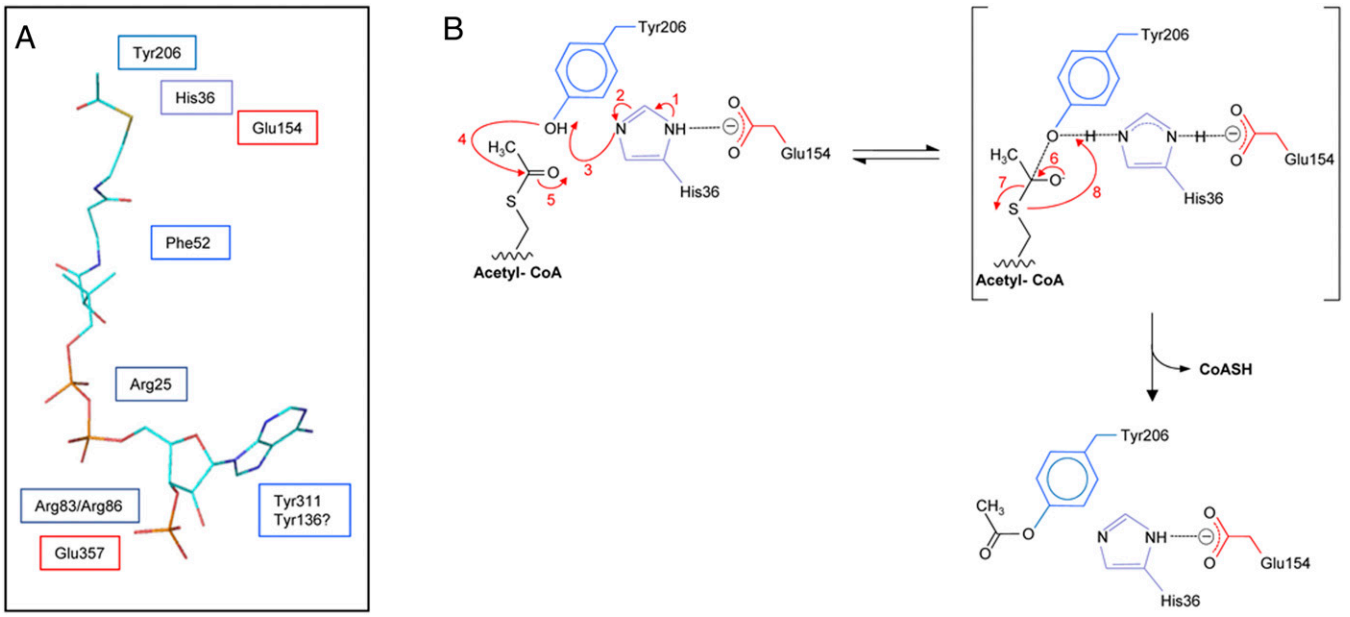

Fig. 5. Proposed binding site of acetyl-CoA and mechanism of action of *Sa*OatA$_N$. (*A*) Proposed positioning of residues identified as essential for *Sa*OatA$_N$ activity relative to acetyl-CoA. The structural conformation of acetyl-CoA presented was adopted from its complex with galactoside acetyltransferase as determined by X-ray crystallography (57) (Protein Data Bank Acc. No. 1KRR). (*B*) Postulated mechanism of *Sa*OatA$_N$. Aided by its interaction with Glu154 (reaction 1, 2; red labeling), His36 acts as a base to abstract the proton from the hydroxyl group of Tyr206 (reaction 3), rendering it nucleophilic. An attack on the carbonyl carbon of the thioester of acetyl-CoA by the nucleophilic Oη of Tyr206 (reaction 4) leads to a putative tetrahedral oxyanion intermediate (reaction 5), which collapses (reaction 6) to release CoASH (reaction 7, 8) and the formation of the *O*-acetyl-Tyr206 product.

adduct and that the acetyl group then migrates to Tyr206. Indeed, an unrelated membrane acetyltransferase, lysosomal heparan sulfate acetyl-CoA:α-glucosaminide *N*-acetyltransferase, was experimentally shown to form an acetyl intermediate on a His residue (59, 60). Our analysis of *Sa*OatA incubated with acetyl-CoA by MALDI-TOF MS did suggest the possibility of three acetyl adducts. However, the MALDI-TOF MS data were not conclusive, and the kinetic data obtained with the various *Sa*OatA variants does not support this mechanism. Typically, the replacement of the catalytic nucleophile with Ala leads to a complete loss of enzymatic activity as observed with (Y206A)*Sa*OatA and previously with OatA$_C$ (32–34), while small amounts of residual activity remain with the replacement of residues providing assistance as detected with the (H36A) and (E154A)*Sa*OatA variants (0.6% and 4.8% residual activity, respectively). Moreover, the replacement of Tyr206 with Ala resulted in a complete abolishment of both esterase and transferase activity; if His36 were the catalytic nucleophile, (Y206A) *Sa*OatA would still be able to function as an esterase.

With Tyr206, His36, and Glu154 of *Sa*OatA$_N$ (*SI Appendix*, Fig. S6) together with Ser453, His578, and Asp575 of *Sa*OatA$_C$ (32) being invariant among all OatA homologs, we propose that the mechanism presented in Fig. 5*B* (and *SI Appendix*, Fig. S11) applies to all OatA enzymes. Moreover, as noted above, a catalytically important His residue homologous to His36 has been identified in the first TMS of all AT-3 proteins. Our alignment of all characterized AT-3 domains fused to SGHN domains for both translocation and the transfer of acetyl groups to extracytoplasmic acceptors indicated that both Glu154 and Tyr206 are also invariant in this subfamily of proteins (*SI Appendix*, Fig. S12). This would suggest that, in addition to all other OatAs, this same mechanism of action applies to other AT-3/SGNH enzymes. The identification and/or assignment of function of the corresponding catalytic nucleophile in the AT-3 domain of the other members of this subfamily of enzymes may have been missed by others given the likely incorrect prediction of topology of the sequence harboring it. Regardless, identification of the catalytic nucleophile of enzymes is key for their further characterization as potential targets for antibacterial development. Indeed, while this subfamily of AT-3 proteins includes hundreds of members, those beyond the Oat enzymes of gram-positive bacteria that have been studied function to modify cell wall glycans in important gram-negative pathogens, such as *N. gonorrhoeae*, *N. meningitidis*, *Haemophilus influenzae*, and species of *Salmonella*.

The location of Tyr206 on an external loop would provide some flexibility for the residue to first function as the nucleophile at the active site of *Sa*OatA$_N$ and then as the acetyl donor for the acetyltransferase reaction at the active site of *Sa*OatA$_C$. Presumably, the two *Sa*OatA domains fold over each other to sandwich a PG acceptor glycan strand between them. This would be consistent with our inability to apply the SCAM method for topology determination as discussed above. Such an association would also explain why the active site of isolated OatA$_C$ appeared to be unusually surface exposed (32–34).

Also, with acetyl-Tyr206 serving as the acetyl donor for OatA$_C$, its binding "site" for this substrate would be, in effect, the entire contact surface area between it and OatA$_N$. As such, OatA$_C$ would be less dependent on discrete binding site/subsites for the productive binding of its substrate *O*-acetyl-Tyr as typical of most other enzymes, including OatA$_N$ for its donor substrate acetyl-CoA. The lack of a discrete binding site would account for the poor binding parameters and virtual lack of specificity observed with *Sa*OatA$_C$ for the model peptides containing *O*-acetyl-Tyr that we tested as substrates in vitro.

Methicillin-resistant *S. aureus* continues to be a major threat, costing the lives of over 10,000 people per year in the United States alone. Hence, there is continued interest in developing new antibiotics for its effective treatment. OatA represents a potential target for antibiotic development, and using this enzyme as a model, this study presents a biochemical characterization of an AT-3 domain. Our findings will help form the basis for further studies of this acetyltransferase and other AT-3 family enzymes with a large array of roles. In particular, our elucidation of the interaction between

the AT-3 and SGNH domains of OatA will inform the search and development of inhibitors as potential antibiotic leads. Indeed, the lack of a discrete binding site for the first half of the acetyltransferase reaction catalyzed by $OatA_C$ has significant ramifications for this search. With the knowledge gleaned from this study, investigators may be better served if in vitro screening assays were designed to target the acceptor half of the reaction. Better still, the application of the in situ assay we developed based on lysozyme sensitivity may prove to be a more effective approach.

Materials and Methods

Bacterial Strains and Growth Conditions. Cultures of bacteria (*SI Appendix*, Table S2) were grown at 37 °C with aeration in Luria-Bertani broth (Difco) or Tryptic Soy broth (TSB) (Difco) as indicated. Media were supplemented with appropriate antibiotics (*E. coli*: 100 μg/mL ampicillin, 50 μg/mL kanamycin; *S. aureus*: 10 μg/mL chloramphenicol) when required.

Cloning, Engineering, and Production of *S. aureus* OatA.
General protocols. Plasmids generated and/or used in this study are listed in *SI Appendix*, Table S3. Custom DNA oligonucleotide primers (*SI Appendix*, Table S4) were obtained from Integrated DNA Technologies. The protocols for the deletion of *oatA* in *S. aureus* USA300 (*S. aureus* USA300 Δ*oatA*) using the method of Bae and Schneewind (61), the cloning of the gene encoding full-length *S. aureus* OatA (residues 1 to 603) (*Sa*OatA), and the generation of *Sa*OatA variants possessing site-specific amino acid replacements by site-directed mutagenesis are described in *SI Appendix, Supplementary Methods*.

Functional Complementation (In Situ) Assay of OatA Variants in *S. aureus*. *S. aureus* USA300 Δ*oatA* was transformed with pACCJ3 carrying the desired mutation. MIC assays were performed with lysozyme in the absence and presence of tunicamycin (0.4 μg/mL) in 200 μL volumes in a 96-well microtitre plate. A 20 h overnight culture of *S. aureus* USA300 Δ*oatA* pACCJ3 was diluted 1/10,000 in sterile TSB. For experiments including tunicamycin, 0.4 μg/mL of the antibiotic (in DMSO) was added such that the final concentration of DMSO was constant at 1% (vol/vol). Filter-sterilized hen egg-white lysozyme (Bio Basic, Inc.) dissolved in water was added at concentrations ranging from 0.25 to 4 mg/mL to each well. Each plate was covered with a Breathe-Easy sealing membrane (Millipore Sigma) and incubated in a Synergy plate reader at 37 °C with double-orbital shaking for 20 h, monitoring optical density at 600 nm every 20 min.

Overproduction and Purification of Full-Length *Sa*OatA and Its Variants. The overproduction of full-length *Sa*OatA and its variants possessing site-specific single amino acid replacements was conducted using E. *coli* C43(DE3) transformed with pACCJ2 or pACCJ2 carrying the desired mutation. The recombinant enzymes were isolated and purified to apparent homogeneity, as determined by SDS-PAGE analysis, by immobilized metal affinity chromatography using fresh resin each time to prevent cross-contamination. Further details are presented in *SI Appendix, Supplementary Methods*. The production and purification of $SaOatA_C$ was performed as described in Jones et al. (32).

Determination of Catalytic Activity and Kinetic Parameters.
As an esterase. Routine determinations of *Sa*OatA and $SaOatA_C$ as an esterase were conducted spectrophotometrically as described previously (32) using 4MU-Ac as substrate in 50 mM sodium phosphate buffer pH 7 containing 5% (vol/vol) DMSO at 25 °C. Unless otherwise stated, all reactions were performed in triplicate, and errors are expressed as SD. Measurements of thioesterase activity toward acetyl-CoA were determined using a modified aldrithiol assay (41) as described in *SI Appendix, Supplementary Methods*.
As a transferase. The MS-based transferase assay previously developed (42) was modified as described in *SI Appendix, Supplementary Methods* to detect the ability of *Sa*OatA to acetylate pseudoacceptors and muroglycans. The muroglycans enzymatically prepared as acceptor substrate had a degree of polymerization (of Lipid II) of 4 to 10 GM-pentapeptides (poly-GM5).

Topology Mapping of $SaOatA_N$ within *Sa*OatA.
SCAM. The protocol of Bogdanov et al. (43) was used in an attempt to determine the topology of $SaOatA_N$ as described in *SI Appendix, Supplementary Methods*.
PhoA-LacZα truncation fusion method. Details for the cloning and engineering of the gene encoding full-length *Sa*OatA (residues 1 to 603) to produce libraries of random exonuclease III–generated truncation fusions to *phoA-lacZα* following the method of Alexeyev and Winkler (44) and their transformation into *E. coli* DH5-α as an α-complementing host strain are presented in *SI Appendix, Supplementary Methods*. Cells were plated on dual indicator plates containing 1.5% (wt/vol) agar, 1% (wt/vol) tryptone, 0.5% (wt/vol) yeast extract, 0.5% (wt/vol) NaCl, 80 mM K_2HPO_4, 80 mg/mL 5-bromo-4-chloro-3-indolyl phosphate disodium salt (Sigma-Aldrich), 100 mg/mL 6-chloro-3-indolyl-β-D-galactopyranoside (Sigma-Aldrich), 1 mM isopropyl β-D-1-thiogalactopyranoside, and 100 μg/mL ampicillin (45). The β-galactosidase and alkaline phosphatase assays were performed as described by Manoil (62) with adaptation to a 96-well plate format (see *SI Appendix* for adaptation methodology and data manipulation).

Identifying In Situ Location of Full-Length *Sa*OatA by Western Blot. The protocol used to detect and locate full-length SaOatA and its variants in transformed strains of *S. aureus* USA300 Δ*oatA* by western immunoblotting (63) is described in *SI Appendix, Supplementary Methods*.

Trapping and Identification of Acetyl-$SaOatA_N$ Intermediate(s). Details for the preparation of samples of *Sa*OatA treated with acetyl-CoA and their MS analyses are described in *SI Appendix, Supplementary Methods*. Briefly, for MALDI-TOF MS, samples were concentrated to 35 μM, washed with 10 mM ammonium acetate, and then mixed with equal volumes of sinapinic acid matrix prior to direct analysis. For LC-MS/MS analyses, reduced and alkylated *Sa*OatA samples were digested with a trypsin/Lys-C mixture followed by MS-grade endoproteinase GluC. The resulting digests were injected directly for LC-MS/MS analysis. To identify sites of any acetylation, the MS/MS data were analyzed using Peaks XPro (Bioinformatics Solutions, Inc.) against the sequences of wild-type *Sa*OatA or (S453A)*Sa*OatA variant according to the protein digested. Variable peptide modifications considered included Asn/Glu deamidation (−0.98 Da), Met oxidation (+15.99 Da), and acetylation of Tyr, His, and/or Ser (+42.01 Da).

Assay of O-Acetylated Tyr-Containing Peptides as Substrate. The synthesis of the O-acetylated peptides, the determination of their concentration, and use as substrates for $SaOatA_C$ are described in *SI Appendix, Supplementary Methods*. Briefly, the specific activity of 5 μM $SaOatA_C$ acting as an esterase toward *O*-acetyl-Tyr–containing peptides was determined spectrophotometrically by monitoring the increase in 278 nm absorbance of peptides (50) in 50 mM sodium phosphate pH 6.5 containing 44% (vol/vol) DMSO.

Other Analytical Techniques. All other analytical techniques used in this study are described in *SI Appendix, Supplementary Methods*.

Data Availability. The raw unprocessed files for *Sa*OatA tryptic peptide LC-MS, corresponding Peaks XPro search results, and annotated MS2 spectra for supporting peptides have been deposited to Figshare (46–48). All other study data are included in the main text and/or *SI Appendix*.

ACKNOWLEDGMENTS. We thank Dr. David Heinrichs, Western University, for his gift of *S. aureus* strains USA300 and RN4220 and plasmids pKOR1 and pALC2073. We also thank Drs. Dyanne Brewer and Armen Charchoglyan of the Mass Spectrometry Facility (Advanced Analysis Centre, University of Guelph) and Valerie Goodfellow (Mass Spectrometry Facility, University of Waterloo) for expert technical assistance and advice and Maria A. Eng, Bryan J. Fraser, Catherine Jany, and Laura Thompson for technical assistance with some of the enzyme assays. These studies were supported in part by operating grants from the Canadian Institutes of Health Research to A.J.C. (TGC 114045) and the Canadian Glycomics Network (https://canadianglycomics.ca/). C.S.J. and A.C.A. were supported in part by graduate scholarships from the Natural Sciences and Engineering Research Council of Canada.

1. S. S. Park, Post-glycosylation modification of sialic acid and its role in virus pathogenesis. *Vaccines (Basel)* **7**, 171 (2019).
2. M. Pauly, V. Ramírez, New insights into wall polysaccharide O-acetylation. *Front. Plant Sci.* **9**, 1210 (2018).
3. V. Sukhithasri, N. Nisha, L. Biswas, V. Anil Kumar, R. Biswas, Innate immune recognition of microbial cell wall components and microbial strategies to evade such recognitions. *Microbiol. Res.* **168**, 396–406 (2013).
4. P. J. Moynihan, A. J. Clarke, O-acetylated peptidoglycan: Controlling the activity of bacterial autolysins and lytic enzymes of innate immune systems. *Int. J. Biochem. Cell Biol.* **43**, 1655–1659 (2011).
5. K. H. Schleifer, O. Kandler, Peptidoglycan types of bacterial cell walls and their taxonomic implications. *Bacteriol. Rev.* **36**, 407–477 (1972).
6. P. J. Moynihan, D. Sychantha, A. J. Clarke, Chemical biology of peptidoglycan acetylation and deacetylation. *Bioorg. Chem.* **54**, 44–50 (2014).

7. E. Bernard *et al*., Characterization of O-acetylation of *N*-acetylglucosamine: A novel structural variation of bacterial peptidoglycan. *J. Biol. Chem.* **286**, 23950–23958 (2011).
8. W. Brumfitt, A. C. Wardlaw, J. T. Park, Development of lysozyme-resistance in *Micrococcus lysodiekticus* and its association with an increased *O*-acetyl content of the cell wall. *Nature* **181**, 1783–1784 (1958).
9. A. Bera, R. Biswas, S. Herbert, F. Götz, The presence of peptidoglycan O-acetyltransferase in various staphylococcal species correlates with lysozyme resistance and pathogenicity. *Infect. Immun.* **74**, 4598–4604 (2006).
10. A. J. Clarke, Extent of peptidoglycan O acetylation in the tribe Proteeae. *J. Bacteriol.* **175**, 4550–4553 (1993).
11. L. Johannsen, H. Labischinski, B. Reinicke, P. Giesbrecht, Changes in the chemical structure of walls of *Staphylococcus aureus* grown in the presence of chloramphenicol. *FEMS Microbiol. Lett.* **16**, 313–316 (1983).
12. S. C. Swim, M. A. Gfell, C. E. Wilde III, R. S. Rosenthal, Strain distribution in extents of lysozyme resistance and O-acetylation of gonococcal peptidoglycan determined by high-performance liquid chromatography. *Infect. Immun.* **42**, 446–452 (1983).
13. J. M. Pfeffer, H. Strating, J. T. Weadge, A. J. Clarke, Peptidoglycan O acetylation and autolysin profile of *Enterococcus faecalis* in the viable but nonculturable state. *J. Bacteriol.* **188**, 902–908 (2006).
14. D. C. Phillips, The hen egg-white lysozyme molecule. *Proc. Natl. Acad. Sci. U.S.A.* **57**, 483–495 (1967).
15. W. Brumfitt, The mechanism of development of resistance to lysozyme by some gram-positive bacteria and its results. *Br. J. Exp. Pathol.* **40**, 441–451 (1959).
16. A. C. Pushkaran *et al*., Understanding the structure-function relationship of lysozyme resistance in *Staphylococcus aureus* by peptidoglycan O-acetylation using molecular docking, dynamics, and lysis assay. *J. Chem. Inf. Model.* **55**, 760–770 (2015).
17. C. Aubry *et al*., OatA, a peptidoglycan *O*-acetyltransferase involved in *Listeria monocytogenes* immune escape, is critical for virulence. *J. Infect. Dis.* **204**, 731–740 (2011).
18. M. Sanchez *et al*., O-acetylation of peptidoglycan limits helper T cell priming and permits *Staphylococcus aureus* reinfection. *Cell Host Microbe* **22**, 543–551.e4 (2017).
19. G. Baranwal *et al*., Impact of cell wall peptidoglycan O-acetylation on the pathogenesis of *Staphylococcus aureus* in septic arthritis. *Int. J. Med. Microbiol.* **307**, 388–397 (2017).
20. A. Bera, S. Herbert, A. Jakob, W. Vollmer, F. Götz, Why are pathogenic staphylococci so lysozyme resistant? The peptidoglycan O-acetyltransferase OatA is the major determinant for lysozyme resistance of *Staphylococcus aureus*. *Mol. Microbiol.* **55**, 778–787 (2005).
21. A. S. Brott, A. J. Clarke, Peptidoglycan O-acetylation as a virulence factor: Its effect on lysozyme in the innate immune system. *Antibiotics (Basel)* **8**, 94 (2019).
22. M. I. Crisóstomo *et al*., Attenuation of penicillin resistance in a peptidoglycan *O*-acetyl transferase mutant of *Streptococcus pneumoniae*. *Mol. Microbiol.* **61**, 1497–1509 (2006).
23. L. Hébert *et al*., *Enterococcus faecalis* constitutes an unusual bacterial model in lysozyme resistance. *Infect. Immun.* **75**, 5390–5398 (2007).
24. F. J. Veyrier *et al*., De-O-acetylation of peptidoglycan regulates glycan chain extension and affects in vivo survival of *Neisseria meningitidis*. *Mol. Microbiol.* **87**, 1100–1112 (2013).
25. T. J. Fleming, D. E. Wallsmith, R. S. Rosenthal, Arthropathic properties of gonococcal peptidoglycan fragments: Implications for the pathogenesis of disseminated gonococcal disease. *Infect. Immun.* **52**, 600–608 (1986).
26. J. K. Blundell, G. J. Smith, H. R. Perkins, The peptidoglycan of *Neisseria gonorrhoeae: O*-acetyl groups and lysozyme sensitivity. *FEMS Microbiol. Lett.* **9**, 259–261 (1980).
27. G. Wang, L. F. Lo, L. S. Forsberg, R. J. Maier, *Helicobacter pylori* peptidoglycan modifications confer lysozyme resistance and contribute to survival in the host. *MBio* **3**, e00409–e00412 (2012).
28. J. Gmeiner, H.-P. Kroll, Murein biosynthesis and O-acetylation of *N*-acetylmuramic acid during the cell-division cycle of *Proteus mirabilis*. *Eur. J. Biochem.* **117**, 171–177 (1981).
29. J. Gmeiner, E. Sarnow, Murein biosynthesis in synchronized cells of *Proteus mirabilis*. Quantitative analysis of O-acetylated murein subunits and of chain terminators incorporated into the sacculus during the cell cycle. *Eur. J. Biochem.* **163**, 389–395 (1987).
30. A. L. Lear, H. R. Perkins, O-acetylation of peptidoglycan in *Neisseria gonorrhoeae*. Investigation of lipid-linked intermediates and glycan chains newly incorporated into the cell wall. *J. Gen. Microbiol.* **132**, 2413–2420 (1986).
31. M. A. Snowden, H. R. Perkins, A. W. Wyke, M. V. Hayes, J. B. Ward, Cross-linking and O-acetylation of newly synthesized peptidoglycan in *Staphylococcus aureus* H. *J. Gen. Microbiol.* **135**, 3015–3022 (1989).
32. C. S. Jones, D. Sychantha, P. L. Howell, A. J. Clarke, Structural basis for the *O*-acetyltransferase function of the extracytoplasmic domain of OatA from *Staphylococcus aureus*. *J. Biol. Chem.* **295**, 8204–8213 (2020).
33. D. Sychantha, A. J. Clarke, Peptidoglycan modification by the catalytic domain of *Streptococcus pneumoniae* OatA follows a ping-pong bi-bi mechanism of action. *Biochemistry* **57**, 2394–2401 (2018).
34. D. Sychantha *et al*., *In vitro* characterization of the antivirulence target of gram-positive pathogens, peptidoglycan O-acetyltransferase A (OatA). *PLoS Pathog.* **13**, e1006667 (2017).
35. H. H. Higa, C. Butor, S. Diaz, A. Varki, O-acetylation and de-O-acetylation of sialic acids. O-acetylation of sialic acids in the rat liver Golgi apparatus involves an acetyl intermediate and essential histidine and lysine residues–A transmembrane reaction? *J. Biol. Chem.* **264**, 19427–19434 (1989).
36. C. R. Pearson *et al*., Acetylation of surface carbohydrates in bacterial pathogens requires coordinated action of a two-domain membrane-bound acyltransferase. *MBio* **11**, e01364–e20 (2020).
37. E. Kintz *et al*., A BTP1 prophage gene present in invasive non-typhoidal *Salmonella* determines composition and length of the O-antigen of the lipopolysaccharide. *Mol. Microbiol.* **96**, 263–275 (2015).
38. F. Thanweer, N. K. Verma, Identification of critical residues of the serotype modifying *O*-acetyltransferase of *Shigella flexneri*. *BMC Biochem.* **13**, 13 (2012).
39. A. Bera *et al*., Influence of wall teichoic acid on lysozyme resistance in *Staphylococcus aureus*. *J. Bacteriol.* **189**, 280–283 (2007).
40. J. Campbell *et al*., Synthetic lethal compound combinations reveal a fundamental connection between wall teichoic acid and peptidoglycan biosyntheses in *Staphylococcus aureus*. *ACS Chem. Biol.* **6**, 106–116 (2011).
41. D. R. Grassetti, J. F. Murray Jr., Determination of sulfhydryl groups with 2,2′- or 4,4′-dithiodipyridine. *Arch. Biochem. Biophys.* **119**, 41–49 (1967).
42. P. J. Moynihan, A. J. Clarke, Assay for peptidoglycan *O*-acetyltransferase: A potential new antibacterial target. *Anal. Biochem.* **439**, 73–79 (2013).
43. M. Bogdanov, W. Zhang, J. Xie, W. Dowhan, Transmembrane protein topology mapping by the substituted cysteine accessibility method (SCAM(TM)): Application to lipid-specific membrane protein topogenesis. *Methods* **36**, 148–171 (2005).
44. M. F. Alexeyev, H. H. Winkler, Membrane topology of the *Rickettsia prowazekii* ATP/ADP translocase revealed by novel dual *pho-lac* reporters. *J. Mol. Biol.* **285**, 1503–1513 (1999).
45. C. Bechara *et al*., MALDI-TOF mass spectrometry analysis of amphipol-trapped membrane proteins. *Anal. Chem.* **84**, 6128–6135 (2012).
46. C. S. Jones, A. Anderson, A. J. Clarke, Full-length SaOatA digest raw MS data. Figshare. https://dx.doi.org/10.6084/m9.figshare.13309427. Deposited 30 November 2020.
47. C. S. Jones, A. Anderson, A. J. Clarke, Full-length SaOatA peptide library search results. Figshare. https://dx.doi.org/10.6084/m9.figshare.13309463. Deposited 30 November 2020.
48. C. S. Jones, A. Anderson, A. J. Clarke, Supporting MS2 spectra for identified acetylpeptides. Figshare. https://dx.doi.org/10.6084/m9.figshare.13309505. Deposited 30 November 2020.
49. M. Sjodt *et al*., Structural coordination of polymerization and crosslinking by a SEDS-bPBP peptidoglycan synthase complex. *Nat. Microbiol.* **5**, 813–820 (2020).
50. J. F. Riordan, B. L. Vallee, [42] o-acetyltyrosine. *Methods Enzymol.* **25**, 500–506 (1972).
51. M. Saidijam, S. Azizpour, S. G. Patching, Comprehensive analysis of the numbers, lengths and amino acid compositions of transmembrane helices in prokaryotic, eukaryotic and viral integral membrane proteins of high-resolution structure. *J. Biomol. Struct. Dyn.* **36**, 443–464 (2018).
52. M. El Ghachi *et al*., Crystal structure of undecaprenyl-pyrophosphate phosphatase and its role in peptidoglycan biosynthesis. *Nat. Commun.* **9**, 1078 (2018).
53. S. D. Workman, L. J. Worrall, N. C. J. Strynadka, Crystal structure of an intramembranal phosphatase central to bacterial cell-wall peptidoglycan biosynthesis and lipid recycling. *Nat. Commun.* **9**, 1159 (2018).
54. R. Dutzler, E. B. Campbell, R. MacKinnon, Gating the selectivity filter in ClC chloride channels. *Science* **300**, 108–112 (2003).
55. D. Ma *et al*., Crystal structure of a membrane-bound *O*-acyltransferase. *Nature* **562**, 286–290 (2018).
56. H. J. Lee *et al*., Structural and kinetic characterizations of the polysialic acid *O*-acetyltransferase OatWY from *Neisseria meningitidis*. *J. Biol. Chem.* **284**, 24501–24511 (2009).
57. X. G. Wang, L. R. Olsen, S. L. Roderick, Structure of the lac operon galactoside acetyltransferase. *Structure* **10**, 581–588 (2002).
58. P. C. Lück *et al*., A point mutation in the active site of *Legionella pneumophila O*-acetyltransferase results in modified lipopolysaccharide but does not influence virulence. *Int. J. Med. Microbiol.* **291**, 345–352 (2001).
59. K. J. Bame, L. H. Rome, Acetyl-coenzyme A:α-glucosaminide N-acetyltransferase. Evidence for an active site histidine residue. *J. Biol. Chem.* **261**, 10127–10132 (1986).
60. S. Durand, M. Feldhammer, E. Bonneil, P. Thibault, A. V. Pshezhetsky, Analysis of the biogenesis of heparan sulfate acetyl-CoA:α-glucosaminide *N*-acetyltransferase provides insights into the mechanism underlying its complete deficiency in mucopolysaccharidosis IIIC. *J. Biol. Chem.* **285**, 31233–31242 (2010).
61. T. Bae, O. Schneewind, Allelic replacement in *Staphylococcus aureus* with inducible counter-selection. *Plasmid* **55**, 58–63 (2006).
62. C. Manoil, Analysis of membrane protein topology using alkaline phosphatase and beta-galactosidase gene fusions. *Methods Cell Biol.* **34**, 61–75 (1991).
63. P. J. Moynihan, A. J. Clarke, O-acetylation of peptidoglycan in gram-negative bacteria: Identification and characterization of peptidoglycan *O*-acetyltransferase in *Neisseria gonorrhoeae*. *J. Biol. Chem.* **285**, 13264–13273 (2010).